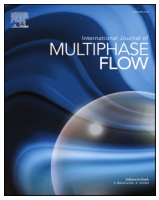
International Journal of Multiphase Flow 194 (2026) 105477



Contents lists available at ScienceDirect

International Journal of Multiphase Flow

journal homepage: www.elsevier.com/locate/ijmulflow





Experimental study on dense-gas/oil flow in horizontal and slightly upward inclined pipes

Carlos Mauricio Ruiz-Diaz [a,*], Cristhian E.A. Pacheco [a], Edson Orati da Silva [a], Gustavo Bochio [a], Alberto T. Postal [b], Oscar M.H. Rodriguez [a]

[a] Industrial Multiphase Flow Laboratory (LEMI), Mechanical Engineering Department, São Carlos School of Engineering (EESC), University of São Paulo (USP), São Carlos, SP, Brazil
[b] Research, Development and Innovation Center (CENPES), Petrobras, Rio de Janeiro, RJ, Brazil

ARTICLE INFO

Keywords:
Gas-liquid flow
Dense gas
Flow patterns
Holdup
Pressure gradient
Experimental data

ABSTRACT

High pressures, critical temperatures, and elevated CO_2 concentrations in ultradeep offshore reservoirs lead to the formation of dense gases within production systems. These conditions result in two-phase flow with dense gas, a flow condition still poorly understood, particularly under slight inclinations. This study presents an extensive experimental investigation of such flow using sulfur hexafluoride (SF_6) and mineral oil in a 2-inch pipeline. A total of 158 data points were obtained under controlled conditions for inclinations of 0°, 5°, and 10°. Holdup was measured using gamma-ray densitometry, and frictional pressure gradients data were evaluated along with flow pattern characterization. The test matrix covered superficial liquid velocities from 0.02 to 2.0 m/s and gas velocities from 0.05 to 1.5 m/s with the liquid-gas density ratio below 10. Transitional flow patterns, i.e., pseudo-slug and dual-continuous, were observed, being the latter atypical in gas-liquid flow. Stratified flow patterns disappeared entirely at inclinations of 5° and 10°, while dispersed flows expanded likely due to inclination-induced phase redistribution. Comparisons with leading commercial simulators highlighted notable discrepancies in holdup and pressure gradient predictions, especially under transitional and stratified flow conditions. These findings underline the need for inclination-aware modeling strategies and offer a valuable experimental database to improve simulator performance in dense-gas/liquid multiphase flows.

1. Introduction

Multiphase flows are of practical and economic importance in the oil and gas industry, particularly in the simultaneous transportation of oil and gas through submarine pipelines installed in ultra-deepwater operations. These pipelines, often operating under various inclinations, transport the mixture to separation facilities under challenging flow and thermodynamic conditions. Two-phase gas-liquid flow is highly prevalent in the extraction of oil and gas in the Brazilian pre-salt fields, particularly under conditions of high gas densities due to specific pressure and temperature conditions (Barreto et al., 2024). The high concentration of CO_2 in the pre-salt fields results in the presence of a high-density gas phase (Carneiro et al., 2015), which in turn leads to significant in-situ volumetric fractions of CO_2 (Li et al., 2025; Yang, 2023). Despite its importance, the behavior of dense-gas/liquid flows remain poorly understood, especially regarding flow patterns, liquid holdup, and pressure gradients under such conditions.

Two-phase flow models and correlations have been usually developed and validated predominantly with air, water, and oil flow data in horizontal, inclined, and vertical pipelines (Barnea, 1987; Rodriguez and Oliemans, 2006; Trallero et al., 1997). When applied to dense-gas/liquid flow conditions, where gas density approaches that of a liquid phase, those models exhibit significant prediction errors (Schmid et al., 2022; Ualiyeva et al., 2022). In ultra-deepwater scenarios, the mismatch between low-density calibration datasets and the elevated-pressure, high-density environments of CO_2-rich flows leads to substantial discrepancies in holdup and frictional pressure-gradient estimates, creating operational risks (Soedarmo et al., 2023).

A substantial body of controlled laboratory investigations has systematically mapped two-phase flow patterns and, through mechanistic analysis, clarified the conditions governing flow pattern transitions. Taitel et al. (1978) proposed mechanistic criteria for pattern formation in horizontal gas-liquid flows within 2 cm and 3 cm i.d. tubes, and Taitel et al. (1980) extended those transition curves to upward air-water flows at 25 °C in vertical pipes of 2.5 cm and 5 cm i.d. Dziubinski et al. (2004)

* Corresponding author.
E-mail address: carlosruiz978@usp.br (C.M. Ruiz-Diaz).

https://doi.org/10.1016/j.ijmultiphaseflow.2025.105477
Received 19 July 2025; Received in revised form 15 September 2025; Accepted 7 October 2025
Available online 8 October 2025
0301-9322/© 2025 Elsevier Ltd. All rights are reserved, including those for text and data mining, AI training, and similar technologies.

List of symbols

A	Cross-sectional area
cps	Counts per second
d	Pipe diameter
D	Dispersed
DC	Dual-continuous
DP	Differential pressure transmitter
Dev	Standard deviation
dP/dz	Pressure gradient
fps	Frames per second
FP	False positive
FN	False negative
g	Gravitational acceleration
GRD	Gamma-ray densitometer
h	Height from the horizontal plane
h	Heigh inside the pipe cross-section
H	Holdup
I	Radiation intensity
l	axial distance between the two pressure taps
L	Length
LEMI	Industrial Multiphase Flow Laboratory
$\dot{m}$	Mass flow rate
ME	Mean error
MAE	Mean absolute error
MRE	Mean relative error
MARE	Mean absolute relative error
q	Quantity in statistical analysis
P	Pressure
PT	Pressure transmitter
PSL	Pseudo-slug
QCV	Quick close valve
RMSRE	Root mean square relative error
SF_6	Sulfur hexafluoride
SL	Slug
ST	Stratified smooth
SW	Stratified wavy
SW/MI	Stratified wavy with mixing at the interface
T	Temperature
TP	True positive
TT	Temperature transmitter
U	Velocity
X	Thickness of the absorbing material

Superscript

$^{+}$	Upstream tap
$^{-}$	Downstream tap

Subscripts

$_{1,\ 2}$	Position
$_{F}$	Frictional
$_{G}$	Gravitational
$_{g}$	Gas phase
$_{i}$	i^{th} experimental point
$_{l}$	Liquid phase
$_{m}$	Mixture
$_{t}$	Dimensional time
$_{T}$	Total

Greek symbol

α	In-situ gas volumetric fraction (void fraction)
ε	Error metric
ϵ	Roughness
Θ	Inclination angle of the pipe
μ	Dynamic viscosity
ρ	Density
σ	Surface tension
γ	Linear absorption coefficient

and Spedding et al. (2003) later compiled comprehensive pattern maps spanning a wide range of inclinations, systematically sowing the interplay between geometry and phase velocities. In flow pattern maps there are transition boundaries upon which characteristics of two flow patterns may coexist and then intermediate behaviors emerge. Many researchers have documented those mixed-pattern zones (Andritsos et al., 1989; Brauner and Ullmann, 2002; De Oliveira et al., 2022; Estivalezes et al., 2022; Ioannou et al., 2005; Tan et al., 2020). A precise characterization of the transition regions, and the associated flow patterns, is essential to assess the reliability of two-phase flow models and enhance their predictive performance across field-related applications (Bazon et al., 2023; Gomez et al., 2023; Li et al., 2018; Osundare et al., 2020; Ruiz-Díaz et al., 2024; Uribe-Tarazona et al., 2025).

Trallero (1995) developed a mechanistic model for liquid-liquid flow pattern transitions that incorporates fluid properties (density, viscosity) and pipe geometry to generate detailed flow-map boundaries based on superficial velocities and holdup. Rodriguez & Oliemans (2006) then validated two-fluid and homogeneous models in a 15 m long, 8.25 cm i.d. loop, using mineral water (ρ= 1000 kg/m^3, $\mu \approx$ 1 mPa·s), oil (ρ= 830 kg/m^3, μ= 7.5 mPa·s), and brine (ρ= 1060 kg/m^3, μ= 0.8 mPa·s), over inclinations from -5° to +5°. Mydlarz-Gabryk et al. (2014) derived analogous equations for water-oil liquid-liquid flows. Mechanistic concepts developed for liquid-liquid flows such as holdup, phase continuity and interfacial topology provide a useful framework for interpreting transitional flow patterns. However, dense-gas/liquid systems differ in key physical respects notably gas compressibility, modified interfacial properties and altered entrainment/drag dynamics, so liquid-liquid correlations and closure relations are not directly transferable. Targeted experiments under high-density gas conditions are therefore required to validate, recalibrate, or extend existing models and to provide the empirical basis needed to adapt mechanistic and empirical approaches to dense-gas/liquid flow.

A lack of dense-gas/liquid two-phase flow data, which underlines the need for accurate experimental investigations. Quintino et al. (2023) provided one of the few datasets for dense-gas/liquid systems, reporting pressure gradients and holdup for six SF_6–oil flow patterns in the horizontal flow direction. Smith et al. (2011) examined slug-dominated behavior in a 69 mm i.d. loop combining SF_6 with low-viscosity and high-viscosity oils. Their measured pressure drop and holdup data agreed relatively well with model predictions in the low-viscosity oil tests, however larger discrepancies were observed using the high-viscosity oils. Khaledi et al. (2014) studied transitions from stratified to intermittent flows at 4 and 8 bara using SF_6 and 100 cP and 32 cP oils, revealing limitations in existing transition models (Smith et al., 2012, 2013). Shmueli et al. (2015) further visualized SF_6, oil, water interfaces in a 69 mm i.d., 50 m horizontal pipe at 0.7 MPa and 20°C, quantifying phase distributions, and compared closure relationships. More recently, Skjæraasen & Kesana (2020) reconstructed liquid-film thickness profiles in a near-horizontal (+2.5°) SF_6-Exxsol D60 flow at 840 kPa, achieving a liquid-to-gas density ratio of approximately 15, yet these experiments still omit steeper inclinations and lower density ratios.

Due to a pronounced lack of experimental data particularly for upward inclinations and liquid-gas density ratios below 10, more studies are required to increase the applicability of classical instability criteria (Bendiksen and Espedal, 1992) and mechanistic models (Taitel and

Dukler, 1976). To address this, the present study systematically investigates slightly upward two-phase flow of SF_6 and mineral oil at a density ratio near 8 in a 2-inch i.d. closed pipe loop, at 0°, 5°, and 10° inclinations. Comprehensive flow-pattern maps, liquid holdup measurements via gamma-ray densitometry, frictional pressure gradients, and captured images by high-speed camera are provided and discussed in the current work. By comparing against existing commercial simulations tools such as Schlumberger's Olga Dynamic Multiphase Flow Simulator and LedaFlow Engineering, these novel data are aimed to improve our understanding about gas-liquid flows of low liquid-gas density ratios and point out some limitations of well-established prediction tools (Jana et al., 2007), often applied to conditions similar to those of ultra-deepwater multiphase transport systems.

2. Methodology and methods

2.1. Experimental facility

The multiphase flow test platform of the Industrial Multiphase Flow Laboratory (LEMI) was used for this study. Fig. 1 shows the schematic diagram of the experimental setup with the more relevant instruments and equipment arrangement. All the designations in this schematic diagram will be used as a reference throughout this document.

The test section is installed on a hydraulically actuated frame that allows inclinations from 0° to 90°; for this study, it was set at 0°, 5°, and 10°. Designed to operate at an absolute pressure of approximately 15 bar. The test section consists of a 52.6 mm ID and 30-meter-long U-shaped pipe. Length-to-diameter ratios (L/d) reported are referenced from the inlet of the U-tube: the differential pressure sensors are at L/d = 88.6, the visualization window at L/d = 131.8, and the pressure/temperature transducers at L/d = 182.2. For reference, these locations correspond to L/d = 221.6, 264.9, and 315.2 when measured from the outlet of the two-phase mixer. Depending on the developing flow pattern, the gas-liquid interface may initiate upstream of the U-tube inlet, even though it reaches its fully developed state only within the test section.

An efficient system for gas-oil separation was designed and installed to handle the two-phase mixture. The two-stage separation process comprises a hydrocyclone and a gravity-driven separator, which are interconnected at both ends by a serpentine that is responsible for reducing the pressure of the substances. Hence, the remaining dispersed or dissolved SF_6 is separated from the oil through a flash process. Subsequently, the oil is pumped from the bottom of the gravitational separator, which also works as oil storage tank, by a helical positive displacement pump and transferred back to the test section, where one of the three volumetric flow meters can be selected for injection. These flow meters operate across different measurement ranges for liquid superficial velocities from 0.008 m/s to 5.5 m/s.

The SF_6 gas phase exiting the separator flows and passes through a fine mesh filter to ensure no liquid droplets enter the storage tank. It is directed to the main compressor, resulting in a pressurized gas, which is then stored in a downstream tank at up to 17 bar absolute pressure to ensure proper delivery to the test section. Upstream the gas inlet to the test section, two control valves regulate the desired mass flow rate, measured with a Coriolis sensor suitable for superficial gas velocities ranging from 0.05 m/s to 4.2 m/s.

An automated control system manages and supervises the experimental sequence. Prior to two-phase operation a single-phase oil run is performed to validate differential-pressure sensors and flow meters and to set the liquid operating point. Liquid flow is maintained by the pump driven through a variable-frequency drive that controls pump RPM to deliver the prescribed volumetric rate in the instrumented section. Gas is supplied from a tank feeding the compressor; this tank is kept at low pressure between 6.5 and 8 bar and the compressor pressurizes gas for downstream storage and delivery to the test line. During data acquisition the compressor remains offline to avoid transient disturbances and the

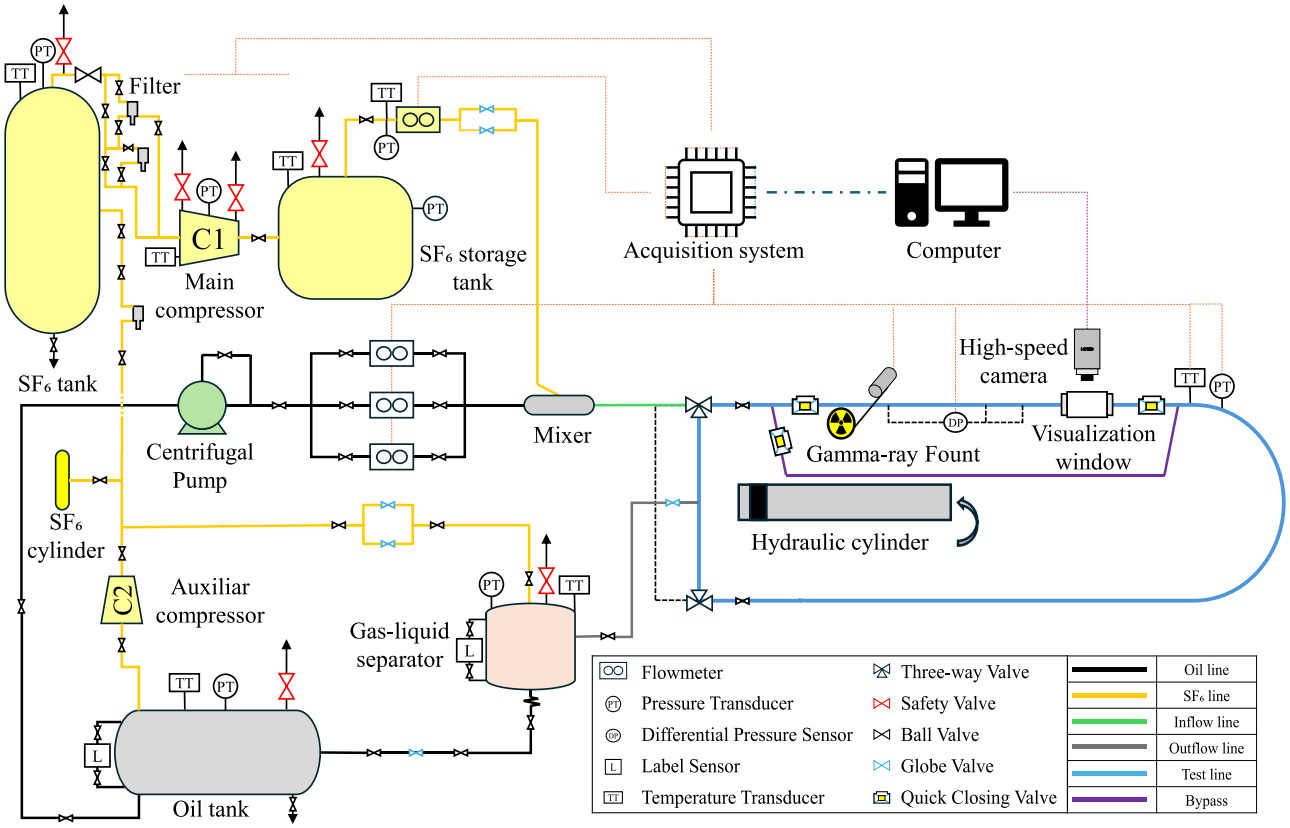


Fig. 1. Schematic diagram of the multiphase flow rig.

test section is supplied from the SF_6 storage tank; gas injection is regulated by a globe valve under PID control that follows the mass-flow setpoint measured by the Coriolis meter. Line pressure is further maintained via valves mounted on the |gas-liquid separator tank, which control the liquid level in the separator and modulate the gas outlet to preserve the target pressure in the pipeline. Transitions between experimental points are effected by updating controller setpoints; the buffer tank, separator valves and valve PID loops preserve line pressure until steady state is re-established, a condition verified prior to beginning data recording.

All piping in the experimental facility is steel, chosen for chemical compatibility with SF_6 and mineral oil and for low internal roughness. Two parallel flexible high-pressure hoses (3 m, rated to 40 bar) are used only in the connections outside the instrumented region for platform inclination.

2.2. Flow loop instrumentation

The measurement and control section, which is located upstream the Mixer (Fig. 1 and Table 1), has the necessary instrumentation for measurement of pressure, temperature, and flow rate separately in each fluid-injection line. The multiphase flow test section, which is located downstream the Mixer (Fig. 2 and Table 1), incorporates the following instrumentation: pressure transducers (PT), temperature transducers (TT), differential pressure transmitters, a visualization window for optical access, a high-speed video camera, quick-closing valves (QCVs), and a gamma-ray densitometer used for void fraction evaluation.

The total pressure gradient is conventionally decomposed into frictional, gravitational and accelerational components, as expressed in Eq. (1), but with the latter neglected due to the constant cross-sectional area (A) and absence of geometric restrictions along the test section. Consequently, under steady-state conditions, the measured pressure gradient predominantly captures the combined effects of frictional resistance and gravitational head.

$$\left(-\frac{dp}{dz}\right)_T = \left(-\frac{dp}{dz}\right)_F + \left(-\frac{dp}{dz}\right)_G \tag{1}$$

Under an inclined flow configuration, the total pressure gradient is determined through the application of Eq. (2).

$$\left(-\frac{dP}{dz}\right)_T = \frac{(P^+ - P^-)}{l} + \alpha\ (\rho_l - \rho_g) g\ sen\Theta + \rho_m\ g\ sen\Theta \tag{2}$$

where $(P^+ - P^-)$ refers to the differential pressure recorded by the differential pressure transmitter, and l represents the axial distance between the two indicated pressure taps (Fig. 3).

The calculation of the frictional pressure gradient is performed using the void fraction (α) obtained via gamma-ray densitometry. The differential pressure measurement is made with capillary tubes filled with oil in order to convey the pressure signal. The gravitational component is evaluated using the mixture density (ρ_m), as defined in Eq. (3).

$$\rho_m = \alpha\rho_g + (1-\alpha)\rho_l \tag{3}$$

The holdup is experimentally determined using a gamma ray densitometer, which features a Cesium-137 source that emits a maximum radiation of 661.6 keV, along with its corresponding photon detector. This detector consists of a scintillation counter LB 5441-03 50/50, equipped with a thallium-doped sodium iodide crystal. This detector exhibits high sensitivity to radiation, ensuring optimal spatial resolution in the experimental measurements. For experiments conducted in the horizontal position, a collimator with a 0.5 mm slit is installed in front of the detector.

The source and detector are mounted on a system that allows different positioning with respect to the pipe, enabling comparative studies to define the optimal positioning. The energy intensity emitted by the source is attenuated by the environment, the pipe material, and the substances flowing inside, with the remaining intensity being quantified by the detector in counts per second (counts/s). To perform these measurements, the instrument must be calibrated in advance. During this calibration, the gas and liquid intensities (power per unit area), I_g and I_l, are determined with the pipe totally filled with gas or liquid, respectively. The phase distribution corresponding to each experimental condition was measured using a control and acquisition system developed in LabVIEW. The acquired data were subsequently processed according to Eq. (4), which represents the attenuation law, commonly referred to as the Lambert–Beer law.

$$I = I_0 e^{(-\gamma X)} \tag{4}$$

In Eq. (4), I represents the transmitted intensity measured by the detector in [counts/s], I_0 is the incident intensity emitted by the radiation source in [counts/s], X is the thickness of the absorbing material in [m], and γ is the linear absorption coefficient in m^{-1}.

From Eq. (4), two additional formulations can be derived to account for the direction of the incident radiation beam on the pipe. These formulations consider the variation in path length and attenuation depending on the beam orientation relative to the pipe geometry, thereby influencing the measured intensities associated with each phase in the two-phase flow. When the beam strikes perpendicularly or at an angle to the fluid interface, as shown in Fig. 4(a), it is expressed by Eq. (5). When the beam is incident parallel to the interface (Álvarez-Pacheco et al., 2024), as illustrated in Fig. 4(b), a simpler linear function can be used, as presented in Eq. (6). These approximations were demonstrated by Stahl & von Rohr (2004).

Table 1
Instrumentation of the measurement and control section and flow test section.

Instrumentation	Brand	Model	Range	Unit	Accuracy
Temperature transmitter[ab]	RÜCKEN	PT 100-TTR-I-100C	0 ~100	°C	± (0.15 + [0.02|T|]°C
Pressure transmitter[ab]	RÜCKEN	Piezoresistive-RTP-420	0 ~2000	kPa	±5 kPa
Differencial pressure transmitter[b]	ENDRESS+HAUSER	PMD75-ABA7FB1BAAA	-40 ~ 40	kPa	±0.1 kPa
Differencial pressure transmitter[b]	ENDRESS+HAUSER	PMD75-ABA7FB1BAAA	-10 ~ 10	kPa	± 0.025 kPa
Differencial pressure transmitter[b]	ENDRESS+HAUSER	PMD75-ABA7DB1BAAA	-3 ~ 3	kPa	± 0.0075 kPa
Coriolis Flow meter[a]	YOKOGAWA	RCEP50S-50BA20-0700-NN00-2-JB1	42 ~3062	kg/h	±0.75% $\dot{m}_g$ for $\dot{m}_g > 670$ kg/h ±(0.9 / $\dot{m}_g$ + 0.602%) for $\dot{m}_g < 670$ kg/h
Turbine flow meter[a]	TECHMETER	TCM-06-IBEA	0.06 ~ 0.6	m^3/h	±0.003 $m^{3/h}$
Turbine flow meter[a]		TCM-15-IBEA	0.4 ~ 8	m^3/h	±0.04 m^3/h
Turbine flow meter[a]		TCM-50-ABEA	2 ~ 40	m^3/h	±0.2 m^3/h

[a] Installed in the measurement and control section.
[b] Installed in the multiphase flow test section.

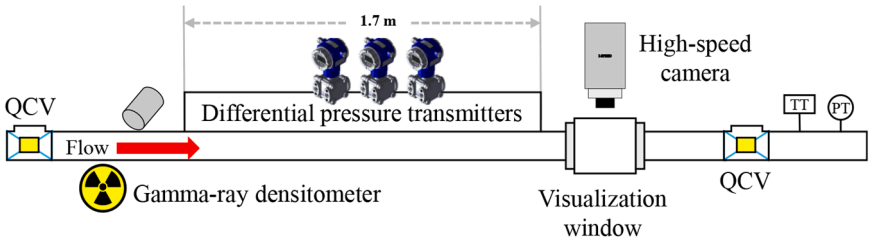


Fig. 2. Schematic of the multiphase flow test section.

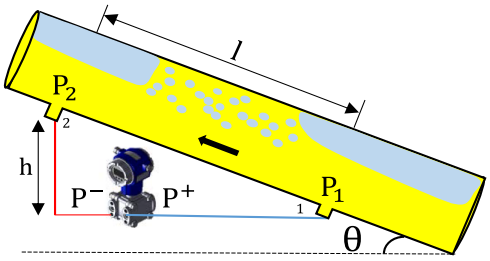


Fig. 3. Schematic of frictional pressure gradient setup for upward two-phase flow.

$$\alpha = \frac{ln\left(\frac{I}{I_l}\right)}{ln\left(\frac{I_g}{I_l}\right)} \tag{5}$$

$$\alpha = \frac{I_l - I}{I_l - I_g} \tag{6}$$

Eq. (7) is used to determine the liquid holdup, H_l, as a function of the void fraction, α.

$$H_l = 1 - \alpha \tag{7}$$

Two QCVs, installed in the multiphase flow test section 8 m apart from each other (Fig. 1), were used to geometrically validate the gamma-ray densitometer data. The maximum deviation was 5 %. The validation measurements were performed under static conditions using Eq. (8).

$$H_l = \frac{1}{4}\left(\pi - \cos^{-1}\left(2\frac{h_l}{d} - 1\right) + \left(2\frac{h_l}{d} - 1\right) \times \sqrt{1 - \left(2\frac{h_l}{d} - 1\right)^2}\right) \tag{8}$$

where h_l represents the liquid heigh observed from the pipe's lateral view, with internal diameter d.

The visualization of flow patterns was carried out through an OLYMPUS I-SPEED 3 SERIES high-speed camera. It was installed at about $L/d \approx 264.9$, where L is the distance from the mixer outlet to the point of measurement. The image acquisition rates were set between 750 and 4000 frames per second (fps), depending on the flow patterns being analyzed.

2.3. Working fluids

For high pressure experiments, sulfur hexafluoride (SF_6) and Turbine X-22 mineral oil were used as the gas and liquid phase, respectively. Their properties within the experimental range are given in Table 2.

A polynomial approximation curve has been fitted to determine the oil viscosity (Eq. (9)) from the experimental results obtained from testing with a HAAKE MARS 3 rheometer, using a 60 mm cone-plate configuration. The tests were conducted across a temperature range of 0.14 °C to 89.97 °C. The Fitted data, however, focus on the 10 °C to 50 °C range, which corresponds to the temperatures at which the oil was experimentally tested.

Table 2
Fluid properties under experimental conditions.

Sulfur hexafluoride - SF_6		Turbine X - 22	
Density (ρ_g)	97.8 ~ 109.8 kg/m^3	Density (ρ_l)	867 kg/m^3
Viscosity (μ_g)	1.68 ~1.73 × 10^{-5} Pa.s	Viscosity (μ_l)	3.01 ~ 5.77 × 10^{-2} Pa.s
Surface tension (σ)		0.032 N/m	
Roughness(ε)		0.000008 m	
Density ratio $\left(\frac{\rho_l}{\rho_g}\right)$		7.89 to 8.87	
Viscosity ratio $\left(\frac{\mu_l}{\mu_g}\right)$		1735.14 to 34040.52	



Fig. 4. Schematic of gamma-ray beam orientations on the pipe cross-section: (a) 45° incidence to the dense-gas/liquid interface, (b) parallel incidence with the source mounted on the vertical displacement system.

$$\mu_l = a * x^b + c \quad \begin{cases} a = 0.5068 & (0.4703,\ 0.5432) \\ b = -0.5774 & (-0.6297,\ -0.525) \\ c = -0.04081 & (-0.0483,\ -0.03332) \end{cases} \tag{9}$$

2.4. Error metrics

The error metrics used to assess the accuracy of the proposed models were the Mean Relative Error (MRE) (ε_1), Mean Absolute Relative Error (MARE) (ε_2) and Root Mean Square Relative Error (RMSRE) (ε_3). ε_1 indicates the average bias of the model, revealing whether it tends to overestimate or underestimate true values. ε_2 measures the average magnitude of relative errors regardless of their direction, providing a straightforward assessment of overall accuracy. Meanwhile, ε_3 applies a quadratic penalty to errors, placing greater emphasis on larger deviations and making it especially sensitive to outliers. Additionally, ε_4, ε_5 correspond to the Mean Error (ME) and Mean Absolute Error (MAE), respectively. Eqs. (10)–(14) detail the error metrics.

$$\boldsymbol{\varepsilon}_1 = \frac{1}{N}\sum_{i=1}^{N}\frac{q_{calculated,i} - q_{measured,i}}{q_{measured,i}} \times 100\% \tag{10}$$

$$\boldsymbol{\varepsilon}_2 = \frac{1}{N}\left|\sum_{i=1}^{N}\frac{q_{calculated,i} - q_{measured,i}}{q_{measured,i}}\right| \times 100\% \tag{11}$$

$$\boldsymbol{\varepsilon}_3 = \sqrt{\frac{1}{N}\sum_{i=1}^{N}\left(\frac{q_{calculated,i} - q_{measured,i}}{q_{measured,i}}\right)^2} \tag{12}$$

$$\boldsymbol{\varepsilon}_4 = \frac{1}{N}\sum_{i=1}^{N}\left(q_{calculated,i} - q_{measured,i}\right) \tag{13}$$

$$\boldsymbol{\varepsilon}_5 = \frac{1}{N}\sum_{i=1}^{N}\left|q_{calculated,i} - q_{measured,i}\right| \tag{14}$$

To evaluate each simulators' ability to classify observed flow patterns, confusion-matrix analysis was employed. Four standard metrics were extracted for every pattern: precision (Eq. (15)), which indicates the fraction of predicted labels that are correct; recall (Eq. (16)), which measures the fraction of actual occurrences that are successfully identified; the F1- score (Eq. (17)), the harmonic mean of precision and recall, which balances false-positive and false-negative rates; and support, the count of true instances of each pattern in the experimental dataset (Eq. (18)).

$$Precision_i = \frac{TP_i}{TP_i + FP_i} \tag{15}$$

$$Recall_i = \frac{TP_i}{TP_i + FN_i} \tag{16}$$

$$F1_i = 2 * \frac{Precision_i * Recall_i}{Precision_i + Recall_i} \tag{17}$$

$$Support_i = TP_i + FN_i \tag{18}$$

2.5. Commercial simulators

For comparison purposes, point models from commercial simulators were employed: LedaFlow 2.11 and both point models available in Olga 2025.1, Olga and Olga HD. Each experimental condition was reproduced in the point models, where the input data consisted of the angle of inclination, liquid and gas superficial velocities, and the phases' viscosities and densities. The pipe inner diameter, roughness, and liquid-gas surface tension were considered constant across all data points. The Olga point models were executed through the Multiphase Toolkit application, and the LedaFlow point model was accessed using the Python API supplied with the simulator. The outputs from the point models compared to experimental data in this study included predicted flow patterns, frictional pressure gradient, and liquid hold-up.

It is important to note that these simulators utilize fewer flow pattern classifications compared to those observed experimentally. Both Olga and Leda include the flow pattern categories Stratified (ST), Stratified Wavy (SW), Annular (A), Slug (SL), and Bubbly (B), while Leda also incorporates Churn (CH). Experimental studies, on the other hand, recognize a broader set of flow patterns, such as Dispersed (D), Dual-continuous (DC), Pseudo Slug (PSL), and Stratified Wavy with Mixing at the Interface (SW/MI). This broader classification underscores the complexity captured in experimental observations compared to the simplifications in the simulators.

3. Results and discussion

3.1. Flow pattern maps

The inclinations were selected to simulate typical operational scenarios in industrial pipelines, capturing the influence of gravitational forces and geometric orientation on the flow dynamics. The experimental dense-gas/liquid flow patterns maps were taken at 0°, 5°, and 10° (Fig. 5). Besides the observation of videos at slow motion, the maps were constructed combining the data analysis of key parameters such as liquid holdup and pressure gradients.

At horizontal inclination (Fig. 5(a)), the map reveals a clear sequence of flow pattern transitions as superficial velocities vary. In the lower-left corner the flow remains stratified smooth (ST), characterized by a stable interface. As U_{sg} increases above 0.2 m/s and at low U_{sl} the interface develops waves, marking the onset of stratified wavy (SW) flow. When U_{sl} reaches 0.5 m/s and U_{sg} is above 0.4 m/s, stratified wavy with mixing at the interface (SW/MI) is observed, where interfacial disruptions and localized entrainment appear. Slug flow (SL) occupies a band at low U_{sg} (0.04-0.15 m/s) and moderate U_{sl} (~ 0.5 m/s), characterized by alternating large gas pockets and liquid slugs. At the highest velocities, U_{sl} near 2 m/s and U_{sg} between 0.5 and 1 m/s, the flow pattern map shows two adjacent flow patterns: dual-continuous (DC), where both phases form continuous interpenetrating layers, and dispersed (D), in which fine gas bubbles are uniformly distributed within the continuous liquid phase. The flow map at 0° is very similar to that presented by Quintino et al. (2023).

Figs. 5(b) and (c) depict the flow pattern maps for inclinations of 5° and 10°, respectively, illustrating both strong similarities and subtle shifts in flow patterns boundaries compared to the horizontal case. Slug flow (SL) is the dominant flow pattern over a broad region, spanning liquid superficial velocities (U_{sl}) from 0.02 to 1.5 m/s and gas superficial velocities (U_{sg}) from 0.05 to 1 m/s. This indicates that slight upward inclinations substantially favor slugging. The pseudo-slug (PSL) flow pattern emerges at moderate U_{sg} ($\approx$ 0.5-1.5 m/s) and low and moderate U_{sl} (0.02-0.7 m/s). At 10°, PSL diminishes at lower U_{sl}, suggesting a shift toward greater slug stability with increasing inclination. Dual-continuous (DC) flow remains localized at the extreme high-velocity region ($U_{sg} > 1.5$ m/s and $U_{sl} > 0.5$ m/s), with its onset shifting slightly toward higher U_{sg} at 10°, reflecting enhanced phase continuity under steeper conditions. Dispersed (D) flow is consistently observed at high U_{sl} (≥ 2 m/s) and over a broad range of U_{sg}. Notably, stratified flow patterns (ST and SW), present at 0°, are completely absent at 5° and 10°, highlighting their sensitivity to even slight upward inclinations. These observations emphasize the robustness of slug flow to inclination.

3.1.1. Flow patterns at 0°

From high-speed camera recordings, each flow pattern was visually identified at 0°, 5°, and 10° inclinations. This qualitative characterization was further reinforced by quantitative analysis of the time-series data of liquid holdup and frictional pressure gradient, which provided

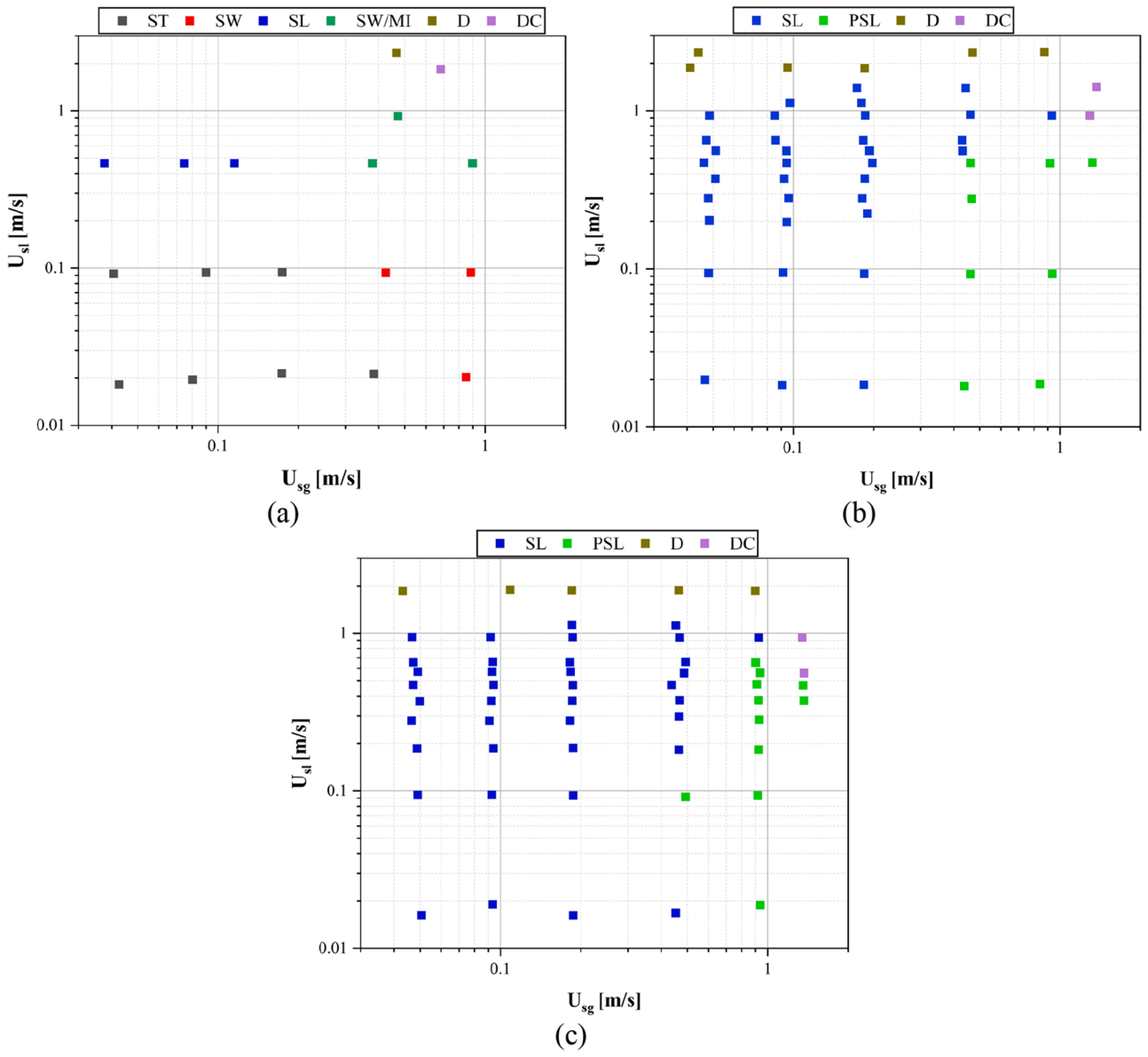


Fig. 5. Experimental flow pattern maps at inclinations of (a) 0°, (b) 5°, and (c) 10°.

objective confirmation of flow pattern stability across the different inclinations. One can see in Fig. 6 the horizontal flow patterns observed. At U_{sg}= 0.38 m/s and U_{sl}= 0.02 m/s (Fig. 6a) a smooth stratified interface (ST) is observed, with minimal wave activity. Increasing U_{sg} to 0.84 m/s and at the same liquid flow induces a wavy stratified pattern (SW, Fig. 6b). When U_{sl} rises to 0.92 m/s at U_{sg}= 0.47 m/s, the interface becomes disrupted and entrainment is observed (SW/MI, Fig. 6c). A classic slug (SL) emerges at U_{sg}= 0.11 m/s and U_{sl}= 0.46 m/s (Fig. 6d), characterized by alternating large gas pockets and liquid slugs. At U_{sg}= 0.68 m/s and U_{sl}= 1.84 m/s, both phases remain continuous, but with very strong entrainment of one phase into the other, in a dual-continuous configuration (DC), an uncommon pattern in gas-liquid flows (Fig. 6e). Finally, at U_{sg}= 0.46 m/s and U_{sl}= 2.33 m/s, dispersed flow pattern (D) with uniform bubble distribution was observed. These observations underscore the critical influence of phase velocities on flow-pattern transitions, and reveal flow patterns such as SW/MI and DC in unexpected regions of the map. Notably, the dual-continuous pattern, previously observed only in liquid-liquid flows, emerged under specific dense-gas/liquid velocity combinations at all three angles, marking it a novel extension of the liquid-liquid flow pattern map described by Rodriguez & Oliemans (2006).

3.1.2. *Flow patterns at 5°, and 10°*

In Fig. 7 there is a comparison of flow patterns observed at 5° (Fig. 7 (a–d)) and 10° (Fig. 7(e–h)) inclinations for selected combinations of gas and liquid superficial velocities, highlighting the evolution of dense-gas/liquid flow behavior under mild upward tilts. In both inclinations, slug flow (SL) is observed at relatively low gas superficial velocities, but in a broad range of liquid superficial velocities.

The main difference observed is that at 10° there is a trend of expansion of SL towards regions of higher gas superficial velocities, which suggests that inclination favors the formation of slug flow. At higher U_{sg} and U_{sl} below 0.7 m/s the pseudo-slug (PSL) dominated the map. PSL is characterized by intermittent flow of high amplitude and wavelength, but non-occlusive, liquid waves. Dual-continuous (DC) flow appears again at the region of highest mixture velocities. At $U_{sg} < 0.9$ m/s and $U_{sl} = 2$ m/s or above dispersed flow (D) dominates. Pipe inclination favors the formation of SL, but at high gas superficial velocities the reverse flow observed at the pipe's bottom side promotes the formation of PSL. It demonstrates that even small increases in inclination can

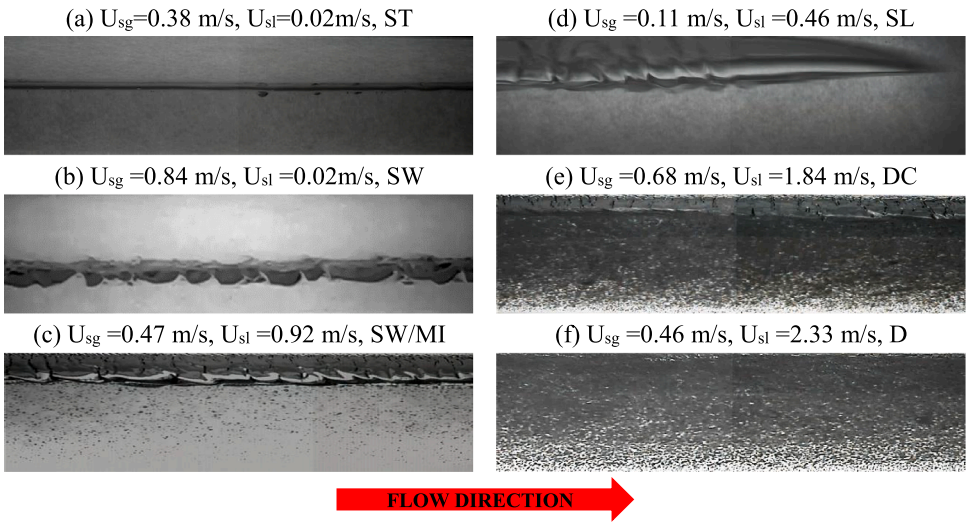


Fig. 6. Flow patterns identified at 0°.

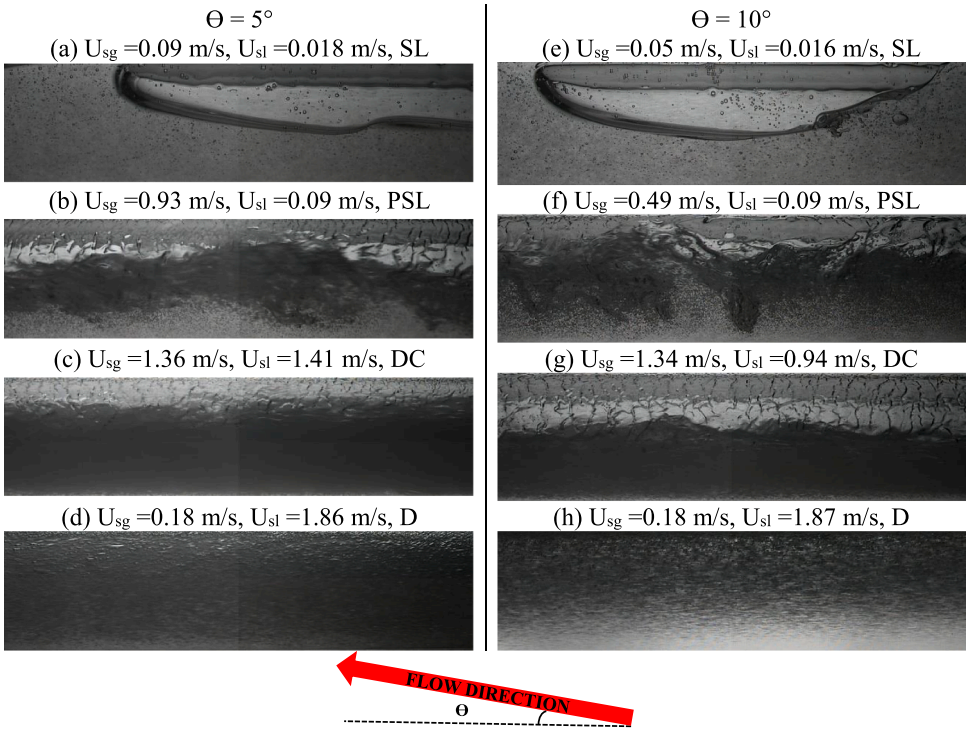


Fig. 7. Flow patterns identified at 5° (a - d), and 10° (e - h).

fundamentally alter the onset, morphology, and stability of dense-gas/liquid flow patterns.

3.2. Flow pattern analysis

Quantitative comparisons between observations and predictions are compiled in Table 3. To harmonize nomenclature, pseudo-slug (PSL) cases were grouped under stratified wavy (SW), and dual-continuous (DC) flow pattern was subsumed into the dispersed (D) category. Across all tested inclinations, Olga 2025.1 delivers the strongest overall classification, with F1 scores of 0.89 for SL, 0.83 for ST, and 0.85 for SW, confirming both high precision and recall in these flow patterns. Olga HD 2025.1 exhibits the weakest performance: it fails entirely to detect ST and DC flows and attains an F1 score of 0.157 for SL, indicating both

Table 3
Overall classification performance metrics for flow pattern.

Simulator	Flow pattern	Precision	Recall	F1-score	Support
Olga 2025.1	D	0.625	0.588	0.606	17
	SL	0.893	0.881	0.887	76
	ST	1.000	0.714	0.833	7
	SW	0.793	0.92	0.851	25
Olga HD 2025.1	D	0.538	0.411	0.466	17
	SL	0.538	0.092	0.157	76
	ST	0	0	0	7
	SW	0.252	1	0.403	25
LedaFlow 2.11	D	0.875	0.411	0.560	17
	SL	0.809	0.447	0.576	76
	ST	0	0	0	7
	SW	0.333	1.000	0.500	25

low sensitivity and high false-positive rates. LedaFlow 2.11 excels in identifying D cases (F1= 0.56) and perfectly recalls SW (recall= 1), but its F1 score for SL reveals a tendency to underpredict this flow pattern, and it similarly misses all ST flow pattern.

The greatest difference in flow regime identification was for experimentally observed slug cases classified as stratified wavy by OLGA HD and LedaFlow. Both OLGA and OLGA HD apply the minimum slip criterion, but OLGA HD computes wall and interface frictions from a two-dimensional velocity distribution, while OLGA relies on bulk layer velocities and empirical friction closures (SLB, 2025). This refinement systematically shifts several slug cases to stratified wavy, as the calculated velocity profile reduces the slip velocity for stratified flow and, consequently, the model's propensity to trigger the slug candidate. LedaFlow also employs a minimum slip criterion, but combines it with a rule-based selection procedure in which slug or churn flow is selected for cases with a consistent solution to the Unit Cell Model (Kongsberg Digital, 2025). As a result, LedaFlow point model underpredicted slug occurrence in borderline cases, particularly at moderate to high gas and liquid velocities.

3.3. Holdup analysis

The maximum absolute uncertainty of the holdup measurements via gamma-ray densitometry remained below 5 % at 0°, associated with stratified wavy flow, and under 14 % at 5° and 10°, associated with slug and pseudo-slug flow patterns, respectively.

Table 4 summarizes the error metrics of holdup prediction using the leading commercial multiphase flow simulators Olga 2025.1, Olga HD 2025.1, and LedaFlow 2.11, with results organized by inclination angle. The performance of each software is evaluated in terms of predictive accuracy, offering critical insights into their reliability and applicability under different flow conditions.

For the horizontal configuration (0°), Olga HD 2025.1 provided the most accurate and consistent quantitative predictions of liquid holdup, exhibiting negligible bias and the lowest RMSRE among the evaluated models. In contrast, Olga 2025.1 showed a systematic overprediction, accompanied by higher scatter, while LedaFlow 2.11 slightly underpredicted holdup and yielded intermediate variability. These results highlight Olga HD 2025.1 as the most reliable model under horizontal flow conditions. At 5° inclination, Olga 2025.1 outperformed the other models, delivering the lowest prediction bias and scatter. Both Olga HD 2025.1 and LedaFlow 2.11 exhibited stronger underprediction and higher RMSRE values. At 10°, Olga 2025.1 again showed superior accuracy, with minimal deviation across all error metrics, while the other models continued to demonstrate significant bias and variability. These results confirm Olga 2025.1 as the most robust option for predicting liquid holdup under slightly upward inclined conditions in dense-gas/liquid flows.

As shown in Fig. 8, which presents holdup data at 0°, 5°, and 10° inclinations, only LedaFlow 2.11 and the Olga version that achieved the best performance are included, based on our prior error-analysis selection. The measured values are contrasted with these simulation predictions to highlight each tool's strengths and limitations, thereby identifying discrepancies and guiding areas for model refinement. Ultimately, these insights support the development of more robust and reliable predictive methods for multiphase flow systems. Fig. 8(a) shows the comparison between measured and predicted liquid holdup values at 0° inclination for Olga HD 2025.1 (filled markers) and LedaFlow 2.11 (open markers), differentiated by flow pattern. Both simulators exhibit reasonable agreement with the equality line, though Olga HD 2025.1 demonstrates superior predictive consistency, with most points falling within the ±20 % error bounds. Notably, Olga HD performs better than LedaFlow in the slug (SL) and dispersed (D) flow patterns, where LedaFlow tends to significantly underpredict holdup. Fig. 8(b) presents the fitted distribution curves of the mean relative error ($\mathcal{E}_1$). The distributions are similar, with Olga HD's distribution slightly narrower and centered closer to zero (peak near -5 %), indicating lower bias and variability. In contrast, LedaFlow's curve is a bit broader, negatively skewed, and peaks around -5 %, confirming a slightly greater tendency toward underestimation. Together, these graphical comparisons support the superior accuracy and robustness of Olga HD 2025.1 in horizontal dense-gas/liquid flow configurations, despite residual challenges in capturing holdup at some stratified flow conditions.

Fig. 8(c) displays the parity plot comparing measured and predicted liquid holdup at 5° inclination for Olga 2025.1 and LedaFlow 2.11. Both simulators exhibit reasonable alignment with the equality line, though with noticeable differences by flow pattern. Olga 2025.1 provides superior accuracy in the slug (SL) and dispersed (D) flow patterns, where its predictions lie predominantly within the ±20 % error bounds. However, pseudo-slug (PSL) and dual-continuous (DC) cases show wider scatter, with systematic underprediction by both tools, more pronounced in LedaFlow. Fig. 8(d) presents the fitted distributions of mean relative error ($\mathcal{E}_1$) for both simulators. Olga 2025.1 exhibits a narrow distribution with its peak centered near -2 %, indicating low bias and moderate dispersion. In contrast, LedaFlow's curve is broader and shifted further left (peak ≈ -5 %), reflecting increased underprediction and variability. These visual cues reinforce the quantitative findings reported earlier, confirming that Olga 2025.1 provides more accurate and consistent holdup predictions under slightly inclined flow conditions.

The performance at 10° inclination is illustrated in Fig. 8(e), where predicted holdup values are plotted against experimental data for Olga 2025.1 and LedaFlow 2.11. The parity plot reveals improved clustering for Olga 2025.1 across all flow patterns, with most points contained within the ±20 % error bounds, especially in slug and pseudo-slug flows. LedaFlow continues to underpredict holdup, particularly in the dispersed and DC flow patterns, where data points deviate significantly below the equality line. Fig. 8(f) shows the corresponding distributions of $\mathcal{E}_1$. Olga's curve is steep, symmetric, and peaks near -2.5 %, suggesting minimal systematic error and tight prediction accuracy. LedaFlow's distribution is broader and centered at -5 %, with heavier tails, indicating greater spread and more pronounced underestimation. Taken together, these figures demonstrate the robustness of Olga 2025.1 at 10° inclination, supporting its use for accurate holdup prediction in dense-gas/liquid flow under mildly inclined conditions.

Table 5 compares the RMSRE ($\mathcal{E}_3$) and its standard deviation (Dev) for each flow pattern, stratified smooth (ST), stratified wavy (SW), stratified wavy with mixing at the interface (SW/MI), slug (SL), pseudo-slug (PSL), dual-continuous (DC), and dispersed (D), across inclinations of 0°, 5°, and 10° for mentioned simulation tools.

Table 4
Comparative error metrics for liquid holdup prediction at 0°, 5°, and 10° inclinations.

Commercial simulator	Θ= 0°					Θ= 5°					Θ= 10°				
	[%]			[-]		[%]			[-]		[%]			[-]	
	$\mathcal{E}_1$	$\mathcal{E}_2$	$\mathcal{E}_3$	$\mathcal{E}_4$	$\mathcal{E}_5$	$\mathcal{E}_1$	$\mathcal{E}_2$	$\mathcal{E}_3$	$\mathcal{E}_4$	$\mathcal{E}_5$	$\mathcal{E}_1$	$\mathcal{E}_2$	$\mathcal{E}_3$	$\mathcal{E}_4$	$\mathcal{E}_5$
Olga 2025.1	5.41	13.60	19.14	0.02	0.07	-1.06	5.07	8.09	-0.01	0.04	-0.28	4.33	5.57	0.00	0.03
Olga HD 2025.1	0.85	12.76	16.95	-0.01	0.07	-5.95	6.26	8.81	-0.04	0.05	-6.65	6.70	7.55	-0.05	0.05
LedaFlow 2.11	1.85	12.94	17.90	0.00	0.07	-6.90	7.07	9.88	-0.05	0.05	-7.39	7.44	9.33	-0.05	0.05

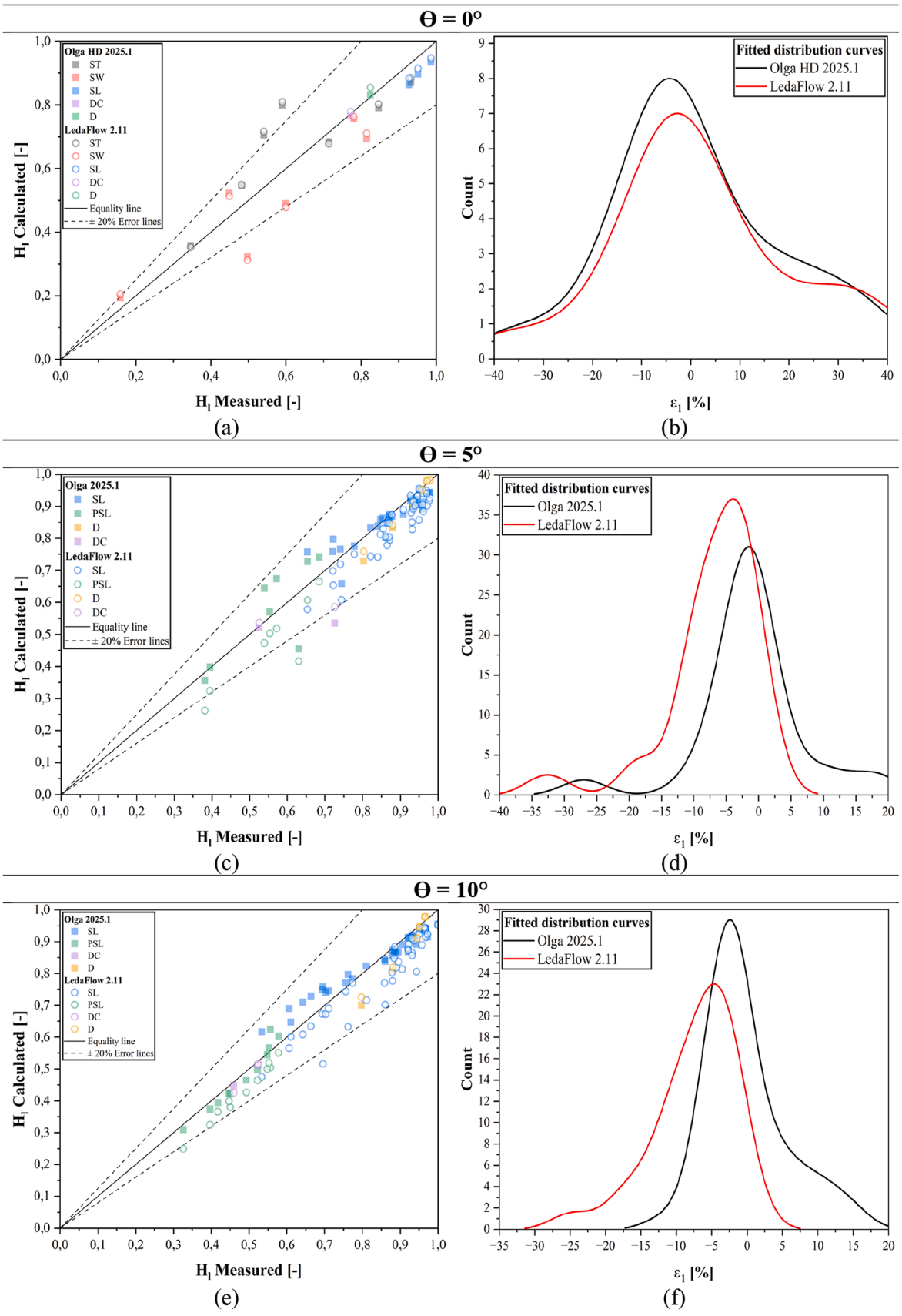


Fig. 8. Liquid holdup results at 0°, 5°, and 10° inclinations: (a, c, e) parity plots by flow pattern; (b, d, f) mean relative error distributions.

Table 5
Error metrics for liquid holdup predictions by flow pattern and inclination.

	$\theta = 0°$						$\theta = 5°$						$\theta = 10°$					
	Olga 2025.1		Olga HD 2025.1		LedaFlow 2.11		Olga 2025.1		Olga HD 2025.1		LedaFlow 2.11		Olga 2025.1		Olga HD 2025.1		LedaFlow 2.11	
	Ɛ3 [%]	Dev [%]	Ɛ3 [%]	Dev [%]	Ɛ3 [%]	Dev [%]	Ɛ3 [%]	Dev [%]	Ɛ3 [%]	Dev [%]	Ɛ3 [%]	Dev [%]	Ɛ3 [%]	Dev [%]	Ɛ3 [%]	Dev [%]	Ɛ3 [%]	Dev [%]
ST	23.94	17.07	18.93	16.41	19.69	16.94	-	-	-	-	-	-	-	-	-	-	-	-
SW	26.06	25.5	26.2	24.02	29.55	27.99	-	-	-	-	-	-	-	-	-	-	-	-
SW/MI	12.96	12.79	12.88	12.87	11.1	11.09	-	-	-	-	-	-	-	-	-	-	-	-
SL	3.49	0.42	5.93	0.71	4.15	0.37	4.77	4.64	5.87	3.74	7	4.08	5.42	5.36	6.44	2.64	8.52	5.32
PSL	-	-	-	-	-	-	14.73	14.33	15.58	9.09	18.81	10.71	5.89	5.63	11.06	2.72	13.2	5.2
DC	0.84	0	0.84	0	0.95	0	18.55	12.76	18.55	12.76	13.71	10.67	2.29	0.14	4.75	2.11	5.25	2.93
D	0.88	0	0.88	0	3.67	0	4.46	3.54	4.45	3.48	3.05	2.34	6.73	4.94	6.73	4.94	5.33	3.78

At 0° inclination, all simulators exhibit their largest RMSRE values in stratified flow patterns, with stratified smooth (ST) and stratified wavy (SW) flows showing the poorest agreement with experimental data. RMSRE values for ST range from 18.9 % (Olga HD) to 23.9 % (Olga 2025.1), while SW errors lie between 26 % and 29.5 %. Notably, the inclusion of interface mixing (SW/MI) improves predictions, reducing RMSRE to below 12.9 %. Olga 2025.1 and LedaFlow both deliver highly accurate predictions in slug flow, with RMSRE values from 3.49 % to 4.15 % and minimal variability. The lowest errors occur in dual-continuous and dispersed flow patterns, where all simulators achieve RMSRE values below 0.95 % and negligible deviation, highlighting their robustness in these well-mixed flow conditions. At 5°, slug flow remains the best-predicted flow pattern across all simulators, with Olga 2025.1 achieving the lowest RMSRE (4.7 %), followed by Olga HD and LedaFlow. Pseudo-slug flow presents significantly higher errors, particularly for LedaFlow, indicating the difficulty of modeling this transitional flow pattern. For dual-continuous and dispersed patterns, LedaFlow provides more accurate predictions, particularly in the dispersed flow pattern where it achieves the lowest RMSRE (3 %). At 10°, Olga 2025.1 consistently outperforms the other tools across most flow patterns, especially in slug, pseudo-slug, and dual-continuous flows, with RMSRE values all below 6.7 %. LedaFlow again demonstrates strong performance in the dispersed flow pattern, while Olga HD shows intermediate results across all patterns.

3.4. Frictional pressure gradient analysis

Table 6 summarizes the comparative performance of the commercial simulators in predicting frictional pressure gradients across all tested inclination angles. Under horizontal conditions (0°), LedaFlow 2.11 demonstrates the most reliable overall performance, achieving the lowest RMSRE ($Ɛ_3$= 38.75 %) and MAE ($Ɛ_5$= 74.09 Pa/m), along with minimal bias ($Ɛ_1$= 0.24 %) and absolute error ($Ɛ_2$= 32.32 %). Although Olga HD 2025.1 exhibits comparable results, LedaFlow's tighter error distribution supports its selection as the most consistent tool for baseline frictional gradient predictions.

At 5° inclination, LedaFlow 2.11 maintains superior accuracy and consistency in predicting the frictional pressure gradient, yielding the lowest RMSRE ($Ɛ_3$= 68.14 %) and MAE ($Ɛ_5$= 279.11 Pa/m). These results outperform both Olga 2025.1 ($Ɛ_3$= 74.45 %, $Ɛ_5$= 304.01 Pa/m) and Olga HD 2025.1 ($Ɛ_3$= 81.69 %, $Ɛ_5$= 335.08 Pa/m). While Olga HD achieves a slightly lower bias ($Ɛ_1$= -1.20 %) than Olga 2025.1 ($Ɛ_1$= 5.96 %), LedaFlow's overall error distribution and reduced absolute deviations support its robustness at mild inclinations. At 10°, Olga 2025.1 emerges as the most balanced predictor, delivering the lowest RMSRE ($Ɛ_3$= 67.88 %) and a competitive MAE ($Ɛ_5$= 166.52 Pa/m). Although Olga HD attains the lowest mean error ($Ɛ_4$= 48.79 Pa/m) and bias ($Ɛ_1$= 2.43 %), its higher scatter ($Ɛ_3$= 88.73 %) reduces its reliability. Thus, Olga 2025.1 is recommended at this inclination due to its improved overall accuracy and reduced dispersion in frictional gradient estimations.

Frictional pressure gradient results are illustrated in Fig. 9, using the same methodology adopted for holdup comparison in Fig. 8. Specifically, only LedaFlow 2.11 and the Olga 2025.1, identified as the most accurate, are considered. Fig. 9(a) shows the parity plot of measured versus predicted frictional pressure gradients at 0° inclination for Olga 2025.1 (filled symbols) and LedaFlow 2.11 (open symbols), categorized by flow pattern. Both simulators generally follow the equality line; however, the largest deviations arise in stratified flow pattern, particularly for stratified smooth (ST) and stratified wavy (SW) cases, where the simulators systematically underestimate the data. For dual-continuous (DC) flows, both models display scatter, although Olga predictions deviate more significantly from the parity line. Fig. 9(b) presents the distributions of mean relative error ($Ɛ_1$). LedaFlow's curve (red) is narrower and more symmetrically centered around zero, reflecting lower bias and variability. In contrast, Olga's distribution (black) is

Table 6
Comparative error metrics for frictional pressure gradient prediction at 0°, 5°, and 10° inclinations.

Commercial Simulator	Θ= 0°					Θ= 5°					Θ= 10°				
	[%]			[Pa/m]		[%]			[Pa/m]		[%]			[Pa/m]	
	ε_1	ε_2	ε_3	ε_4	ε_5	ε_1	ε_2	ε_3	ε_4	ε_5	ε_1	ε_2	ε_3	ε_4	ε_5
Olga 2025.1	0.24	34.42	43.78	96.83	109.04	5.96	54.95	74.45	119.90	304.01	6.21	45.93	67.88	43.61	166.52
Olga HD 2025.1	2.28	36.73	47.13	100.15	112.20	-1.2	61.71	81.69	109.63	335.08	2.43	48.15	88.73	48.79	161.16
LedaFlow 2.11	1.40	32.32	38.75	63.20	74.09	-12	51.87	68.14	27.28	279.11	-4.9	45.72	72.90	-0.91	162.04

wider and slightly shifted toward positive values, indicating a tendency to overpredict. The narrower error bounds and reduced scatter observed for LedaFlow, particularly in SW, ST, and DC flow patterns, highlight its reliability and establish it as the preferred simulator for predicting frictional pressure gradients under horizontal flow conditions.

Fig. 9(c) presents the parity plot comparing measured and predicted frictional pressure gradients for Olga 2025.1 and LedaFlow 2.11 at 5° inclination. Both simulators capture the overall trend but suffer their greatest deviations in the slug (SL) and pseudo-slug (PSL) flow patterns. Many SL/PSL points lie outside the ±40 % error bounds, and the dispersed (D) cases at high liquid velocities also display significant scatter. Quantitatively, LedaFlow 2.11 achieves the lowest overall scatter (RMSRE) and smallest absolute deviations (MAE), outperforming Olga 2025.1. The corresponding error distributions in Fig. 9(d) reinforce these findings: Olga's curve is wide and skewed positive evidence of systematic overprediction, while LedaFlow's distribution, though narrower, remains offset, highlighting underprediction in SL, PSL, and D flow patterns. These results indicate that LedaFlow 2.11 offers the best balance of precision and consistency at 5°. Fig. 9(e) presents the parity comparison for Olga 2025.1 and LedaFlow 2.11, at 10° inclination. Olga's predictions predominantly fall within the ±40 % error bounds, while LedaFlow tends to overpredict, particularly in the dispersed (D) flow pattern. As shown in Fig. 9(f), Olga's error distribution is narrower and centered closer to zero, whereas LedaFlow's is broader and positively skewed. These visual trends are consistent with the numerical indicators: Olga 2025.1 exhibits the lowest RMSRE and a competitive MAE, surpassing both Olga HD 2025.1 and LedaFlow in overall accuracy and scatter. Although Olga HD displays the lowest mean error and bias, Olga 2025.1′s tighter error distribution and reduced variability make it the most reliable tool for frictional pressure gradient predictions at steeper inclinations.

Table 7 reveals that frictional pressure gradient prediction errors exhibit strong dependency on flow pattern and inclination. Under horizontal conditions (0°), stratified flow pattern, including ST, SW, and SW/MI, consistently yield the highest RMSREs, with Olga versions exceeding 49.9 % and LedaFlow reaching 37.0 %, indicating persistent model limitations in these flow patterns. In contrast, slug flow is predicted with moderate accuracy, with LedaFlow (RMSRE= 23.25 %, Dev= 5.94 %) outperforming Olga 2025.1 and Olga HD. Dispersed flow pattern is best captured by LedaFlow (RMSRE= 6.01 %), while dual-continuous flow shows extreme deviations in Olga (RMSRE= 78.85 %).

At 5°, slug and pseudo-slug predictions deteriorate significantly, with RMSREs exceeding 50 % and 70 %, respectively. Dispersed flow error rises sharply for Olga 2025.1 (152.79 %), but remains comparatively lower for LedaFlow (69.82 %), underscoring its robustness. At 10°, moderate improvements are observed in slug and DC predictions, but pseudo-slug and dispersed flows remain challenging. These trends highlight that stratified and transitional patterns (pseudo-slug and dual-continuous) remain the most difficult to predict reliably, suggesting the need for enhanced model formulations targeting such flow patterns.

4. Conclusions

A novel experimental apparatus was developed to investigate dense-gas/liquid two-phase flow under horizontal and slightly upward inclined conditions, yielding 158 data points for a liquid-gas density ratio of about 8. The results revealed complex hydrodynamic behaviors, most notably the emergence of pseudo-slug and dual-continuous flow patterns at low inclinations, which demonstrate ambiguous characteristics between gas-liquid and liquid-liquid flows depending on flow conditions.

Flow pattern predictions indicate that while Olga 2025.1 is the best general choice, LedaFlow 2.11 should be used when dispersed or stratified wavy flows are the focus. The overall failure to detect dual-continuous flows across all tools highlights a clear need to improve model representations of continuous interpenetrating phases.

Comparative evaluation of commercial simulators showed notable limitations in holdup and frictional pressure gradient predictions, particularly under stratified and transitional flow patterns. Among the tested models, Olga HD 2025.1 exhibited the highest accuracy under horizontal conditions, especially in stratified smooth and wavy patterns, and produced the most consistent frictional gradient estimates. For upward inclined configurations (5° and 10°), Olga 2025.1 demonstrated superior performance in predicting holdup for slug, pseudo-slug, and dual-continuous flow patterns, and emerged as the preferred option for frictional gradient estimation at steeper inclinations.

LedaFlow 2.11 was found to be more reliable in flow patterns characterized by high mixing and dispersion, such as dispersed and dual-continuous flows, providing competitive results for both holdup and pressure gradient under slightly inclined conditions. Nevertheless, its performance declined in stratified configurations. Across all tools and inclinations, the most significant discrepancies occurred in stratified and transitional flow patterns, highlighting the need for improved interfacial and entrainment modeling in dense-gas/liquid systems.

The findings underscore the necessity for further model refinement to improve predictive capabilities. The experimental database generated in this work provides a valuable benchmark for validation and development of multiphase flow models, particularly for dense-gas/liquid flows.

CRediT authorship contribution statement

Carlos Mauricio Ruiz-Diaz: Writing – review & editing, Writing – original draft, Visualization, Validation, Methodology, Investigation, Formal analysis, Data curation, Conceptualization. **Cristhian E.A. Pacheco:** Writing – review & editing, Visualization, Methodology, Investigation, Formal analysis, Data curation. **Edson Orati da Silva:** Writing – review & editing, Visualization, Methodology, Investigation, Formal analysis, Data curation. **Gustavo Bochio:** Writing – review & editing, Visualization, Validation, Resources, Project administration, Methodology, Formal analysis. **Alberto T. Postal:** Writing – review & editing, Validation, Software, Resources, Project administration, Funding acquisition. **Oscar M.H. Rodriguez:** Writing – review & editing, Supervision, Resources, Project administration, Formal analysis, Conceptualization.

Declaration of competing interest

The authors declare that they have no known competing financial interests or personal relationships that could have appeared to influence

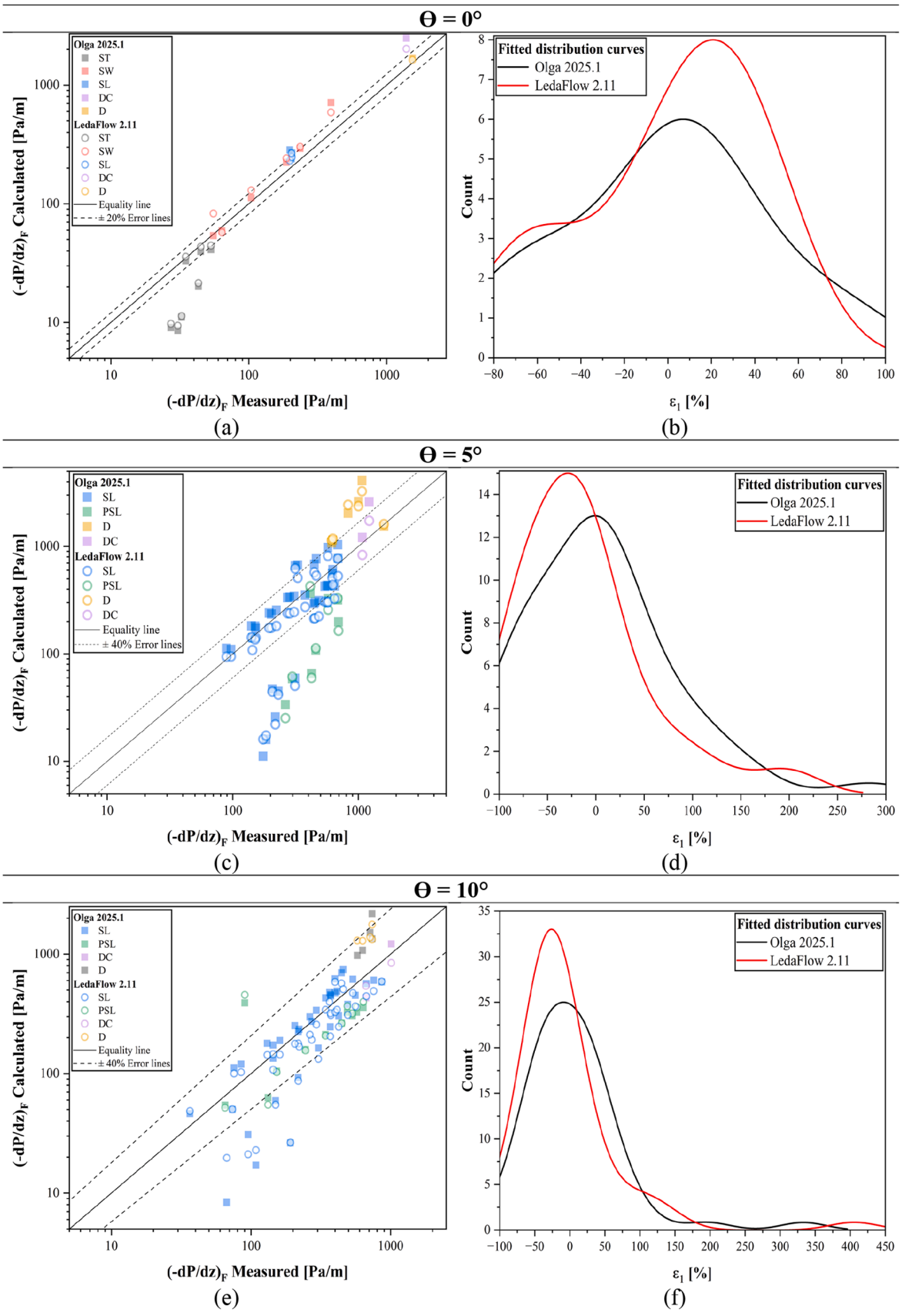


Fig. 9. Frictional pressure gradient results at 0°, 5°, and 10° inclinations: (a, c, e) parity plots by flow pattern; (b, d, f) mean relative error distributions.

Table 7
Error metrics for frictional pressure gradient predictions by flow pattern and inclination.

	$\theta = 0°$						$\theta = 5°$						$\theta = 10°$					
	Olga 2025.1		Olga HD 2025.1		LedaFlow 2.11		Olga 2025.1		Olga HD 2025.1		LedaFlow 2.11		Olga 2025.1		Olga HD 2025.1		LedaFlow 2.11	
	ε_3 [%]	Dev [%]	ε_3 [%]	Dev [%]	ε_3 [%]	Dev [%]	ε_3 [%]	Dev [%]	ε_3 [%]	Dev [%]	ε_3 [%]	Dev [%]	ε_3 [%]	Dev [%]	ε_3 [%]	Dev [%]	ε_3 [%]	Dev [%]
ST	49.99	26.36	50.84	25.18	47.76	29.02	-	-	-	-	-	-	-	-	-	-	-	-
SW	6.55	6.5	21.63	13.88	32.62	24.57	-	-	-	-	-	-	-	-	-	-	-	-
SW/MI	49.88	27.77	68.07	23.57	37.05	9.9	-	-	-	-	-	-	-	-	-	-	-	-
SL	32.08	10.64	9.43	6.68	23.25	5.94	51.46	51.44	61.87	59.67	48.36	42.12	40.63	40.5	42.73	36.59	38.58	31.94
PSL	-	-	-	-	-	-	68	24.35	66.34	37.18	69.92	28.37	107.02	106.94	161.55	158.45	127.51	127.46
DC	78.85	0	78.85	0	45.72	0	80.45	50.31	80.45	50.31	33.69	32.25	28.9	27.96	14.64	9.67	17.46	0.94
D	10.08	0	10.08	0	6.01	0	152.79	88.78	162.38	86.61	137.58	69.82	116.33	47.9	129.61	45.66	111.03	21.28

the work reported in this paper.

Acknowledgements

The authors would like to thank Petrobras and ANP for the financial support. Oscar Rodriguez would like to thank CNPq for the productivity grant (proc. 311057/2020-9). Carlos Ruiz gratefully acknowledges the support of the Ministerio de Ciencia, Tecnología e Innovación of Colombia.

Data availability

Data will be made available on request.

References

Álvarez-Pacheco, C.E., Ruiz-Diaz, C.M., Hernandez-Rodriguez, O.M., 2024. Chordal measurement of phase fraction distribution in a static gas-liquid system using collimated gamma-ray densitometer and artificial neural networks. Rev. Ingenio 21 (1), 29–35. https://doi.org/10.22463/2011642X.4098.

Andritsos, N., Williams, L., Hanratty, T.J., 1989. Effect of liquid viscosity on the stratified-slug transition in horizontal pipe flow. Int. J. Multiph. Flow 15 (6), 877–892. https://doi.org/10.1016/0301-9322(89)90017-7.

Barnea, D., 1987. A unified model for predicting flow-pattern transitions for the whole range of pipe inclinations. Int. J. Multiph. Flow 13 (1), 1–12. https://doi.org/10.1016/0301-9322(87)90002-4.

Barreto, C.V., Ramos, C.S., Bocchi, G., Trujillo, J., Pasqualette, M., Carneiro, J., Costa, F., & Graciano, J. (2024). Flow assurance applied to CO2 transport: challenges of modelling CO2-rich systems through production, processing and injection systems. 2 (June 2025), 1–11. https://doi.org/10.4043/35146-ms.

Bazon, P.B., Castro-Bolivar, J.E., Ruiz-Diaz, C.M., Hernández-Cely, M.M., Rodriguez, O. M.H., 2023. Hybrid machine learning model applied to phase inversion prediction in liquid-liquid pipe flow. Multiph. Sci. Technol. 35 (1), 35–53. https://doi.org/10.1615/MultScienTechn.2022046139.

Bendiksen, K., Espedal, M., 1992. Onset of slugging in horizontal gas-liquid pipe flow. Int. J. Multiph. Flow 18 (2), 237–247. https://doi.org/10.1016/0301-9322(92)90086-V.

Brauner, N., Ullmann, A., 2002. Modeling of phase inversion phenomenon in two-phase pipe flows. Int. J. Multiph. Flow 28 (7), 1177–1204. https://doi.org/10.1016/S0301-9322(02)00017-4.

Carneiro, J.N.E., Pasqualette, M.A., Reyes, J.F.R., Krogh, E., Johansen, S.T., Ciambelli, J. R.P., Rodrigues, H.T., Fonseca, R., 2015. Numerical simulations of high CO2 content flows in production wells, flowlines and risers. OTC Bras. 1522–1533. https://doi.org/10.4043/26231-MS. *June 2025*.

De Oliveira, M.R., Martins, M.F., Belich, H., Amorim, L., 2022. A model for predicting two-phase flow patterns transitions in an annulus: inclinations from horizontal to near-vertical. Chem. Eng. Sci. 250, 117379. https://doi.org/10.1016/j.ces.2021.117379.

Dziubinski, M., Fidos, H., Sosno, M., 2004. The flow pattern map of a two-phase non-Newtonian liquid-gas flow in the vertical pipe. Int. J. Multiph. Flow 30 (6), 551–563. https://doi.org/10.1016/j.ijmultiphaseflow.2004.04.005.

Estivalezes, J.L., Aniszewski, W., Auguste, F., Ling, Y., Osmar, L., Caltagirone, J.P., Chirco, L., Pedrono, A., Popinet, S., Berlemont, A., Magnaudet, J., Ménard, T., Vincent, S., Zaleski, S., 2022. A phase inversion benchmark for multiscale multiphase flows. J. Comput. Phys. 450, 110810. https://doi.org/10.1016/j.jcp.2021.110810.

Gomez, C., Ruiz, D., Cely, M., 2023. Specialist system in flow pattern identification using artificial neural networks. J. Appl. Eng. Sci. 21 (2), 285–299. https://doi.org/10.5937/jaes0-40309.

Ioannou, K., Nydal, O.J., Angeli, P., 2005. Phase inversion in dispersed liquid–liquid flows. Exp. Therm. Fluid Sci. 29 (3), 331–339. https://doi.org/10.1016/j.expthermflusci.2004.05.003.

Jana, A.K., Ghoshal, P., Das, G., Das, P.K., 2007. An analysis of pressure drop and holdup for liquid-liquid upflow through vertical pipes. Chem. Eng. Technol. 30 (7), 920–925. https://doi.org/10.1002/ceat.200700033.

Khaledi, H.A., Smith, I.E., Unander, T.E., Nossen, J., 2014. Investigation of two-phase flow pattern, liquid holdup and pressure drop in viscous oil-gas flow. Int. J. Multiph. Flow 67, 37–51. https://doi.org/10.1016/j.ijmultiphaseflow.2014.07.006.

Kongsberg Digital, 2025. LedaFlow 2.11 User Man.

Li, C., Liao, Y., Jia, W., Yang, F., He, J., Wang, X., 2025. A two-fluid model incorporating droplet entrainment to predict pressure drop and holdup for CO2 two-phase flow in horizontal and vertical pipe. J. Pipeline Sci. Eng., 100304 https://doi.org/10.1016/j.jpse.2025.100304.

Li, Z., Wang, G., Yousaf, M., Yang, X., Ishii, M., 2018. Flow structure and flow regime transitions of downward two-phase flow in large diameter pipes. Int. J. Heat Mass Transf. 118, 812–822. https://doi.org/10.1016/j.ijheatmasstransfer.2017.11.037.

Mydlarz-Gabryk, K., Pietrzak, M., Troniewski, L., 2014. Study on oil–water two-phase upflow in vertical pipes. J. Pet. Sci. Eng. 117, 28–36. https://doi.org/10.1016/j.petrol.2014.03.007.

Osundare, O.S., Falcone, G., Lao, L., Elliott, A., 2020. Liquid-Liquid flow pattern prediction using relevant dimensionless parameter groups. Energies 13 (17), 4355. https://doi.org/10.3390/en13174355.

Quintino, A.M., da Fonseca Junior, R., Rodriguez, O.M.H., 2023. Experimental study of liquid/dense-gas pipe flow. Geoenergy Sci. Eng. 230, 212179. https://doi.org/10.1016/j.geoen.2023.212179. July.

Rodriguez, O.M.H., Oliemans, R.V.A., 2006. Experimental study on oil–water flow in horizontal and slightly inclined pipes. Int. J. Multiph. Flow 32 (3), 323–343. https://doi.org/10.1016/j.ijmultiphaseflow.2005.11.001.

Ruiz-Díaz, C.M., Quispe-Suarez, B., González-Estrada, O.A., 2024. Two-phase oil and water flow pattern identification in vertical pipes applying long short-term memory networks. Emergent Mater. 7 (5), 1983–1995. https://doi.org/10.1007/s42247-024-00631-2.

Schmid, D., Verlaat, B., Petagna, P., Revellin, R., Schiffmann, J., 2022. Flow pattern observations and flow pattern map for adiabatic two-phase flow of carbon dioxide in vertical upward and downward direction. Exp. Therm. Fluid Sci. 131, 110526. https://doi.org/10.1016/j.expthermflusci.2021.110526. July 2021.

Shmueli, A., Unander, T.E., Nydal, O.J., 2015. Characteristics of gas/water/viscous oil in stratified-annular horizontal pipe flows. OTC Bras. https://doi.org/10.4043/26176-MS. D021S024R004.

Skjæraasen, O., Kesana, N.R., 2020. X-ray measurements of thin liquid films in gas–liquid pipe flow. Int. J. Multiph. Flow 131, 103391. https://doi.org/10.1016/j.ijmultiphaseflow.2020.103391.

SLB, 2025. OLGA 2025,1 User Man.

Smith, I.E., Krampa, F.N., Fossen, M., Brekken, C., Unander, T.E., 2011. Investigation of horizontal two-phase gas-liquid pipe flow using high viscosity oil: comparison with experiments using low viscosity oil and simulations. In: 15th International Conference on Multiphase Production Technology. BHR-2011-G3.

Smith, I.E., Nossen, J., Erling Unander, T., 2013. Improved holdup and pressure drop predictions for multiphase flow with gas and high viscosity oil. In: 16th International Conference on Multiphase Production Technology. BHR-2013-C4.

Smith, I.E., Schlegel, J.P., Hibiki, T., Ishii, M., 2012. Two-phase flow structure in large diameter pipes. Int. J. Heat Fluid Flow 33 (1), 156–167. https://doi.org/10.1016/j.ijheatfluidflow.2011.10.008.

Soedarmo, A.A., Pereyra, E., Sarica, C., 2023. Performance mapping of multiphase flow model – connecting the dots from experimental data. Day 4 Thu. https://doi.org/10.4043/32170-MS. *May 0420232023-May*.

Spedding, P.L., Cooper, R.K., Mcbride, W.J., 2003. A universal flow regime map for horizontal Two-Phase flow in pipes. Dev. Chem. Eng. Min. Proc. 11 (1–2), 95–106. https://doi.org/10.1002/apj.5500110209.

Stahl, P., von Rohr, P.R., 2004. On the accuracy of void fraction measurements by single-beam gamma-densitometry for gas-liquid two-phase flows in pipes. Exp. Therm. Fluid Sci. 28 (6), 533–544. https://doi.org/10.1016/j.expthermflusci.2003.08.003.

Taitel, L., N, Dukler, A.E, 1978. Transient gas-liquid flow in horizontal pipes: modeling the flow pattern transitions. AIChE J. 24 (5), 920–934. https://doi.org/10.1002/aic.690240518.

Taitel, Y., Barnea, D., Dukler, A.E., 1980. Modelling flow pattern transitions for steady upward gas-liquid flow in vertical tubes. AIChE J. 26 (3), 345–354. https://doi.org/10.1002/aic.690260304.

Taitel, Y., Dukler, A.E., 1976. A model for predicting flow regime transitions in horizontal and near horizontal gas-liquid flow. AIChE J. 22 (1), 47–55. https://doi.org/10.1002/aic.690220105.

Tan, J., Luo, P., Vahaji, S., Jing, J., Hu, H., Yu, B., Tu, J., 2020. Experimental investigation on phase inversion point and flow characteristics of heavy crude oil-water flow. Appl. Therm. Eng. 180, 115777. https://doi.org/10.1016/j.applthermaleng.2020.115777. July.

Trallero, J.L., 1995. Oil–Water flow Patterns In Horizontal Pipes. The University of Tulsa, Tulsa, Oklahoma.

Trallero, J.L., Sarica, C., Brill, J.P., 1997. A study of oil/water flow patterns in horizontal pipes. SPE Prod. Facil. 12 (03), 165–172. https://doi.org/10.2118/36609-PA.

Ualiyeva, G., Pereyra, E., Sarica, C., 2022. An experimental study on two-phase downward flow of medium viscosity oil and air. In: Proceedings - SPE Annual Technical Conference and Exhibition. https://doi.org/10.2118/209969-MS. *2022-Octob*.

Uribe-Tarazona, D.Y., Ruiz-Diaz, C.M., González-Estrada, O.A., 2025. Machine learning technique for the identification of two-phase (oil-water) flow patterns through pipelines. Front. Mech. Eng. 11. https://doi.org/10.3389/fmech.2025.1522120.

Yang, Z., 2023. A study of CO2 two-phase flow in a near horizontal pipe. J. Pipeline Sci. Eng. 3 (2), 100106. https://doi.org/10.1016/j.jpse.2022.100106.